Self-aggregation, dilational surface rheology and foaming properties of 1-O-dodecyl diglyceryl ether compared to n-dodecyl-β-D-maltoside and pentaethyleneglycol monododecyl ether

Lucie Delforce, Véronique Rataj, Raphael Lebeuf, Jean-Marie Aubry, Jesus Ontiveros

Self-aggregation, dilational surface rheology and foaming properties of 1-*O*-dodecyl diglyceryl ether compared to *n*-dodecyl-β-D-maltoside and pentaethyleneglycol monododecyl ether

Lucie Delforce, Véronique Nardello-Rataj, Raphaël Lebeuf, Jean-Marie Aubry, Jesús Fermín Ontiveros*

Univ. Lille, CNRS, Centrale Lille, Univ. Artois, UMR 8181 - UCCS – Unité de Catalyse et Chimie du Solide, F-59000 Lille, France

jesus-fermin.ontiveros@centralelille.fr

Graphical Abstract

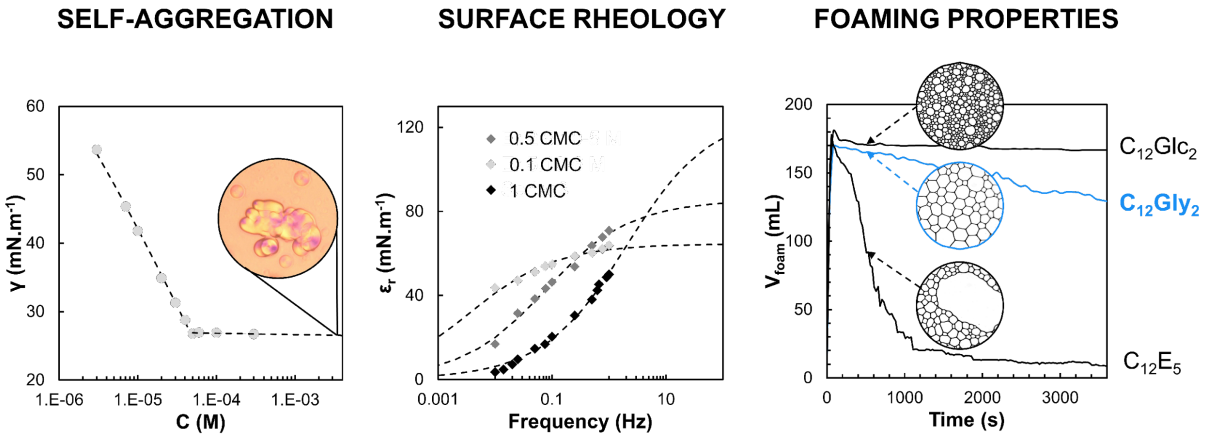

Abstract

Diglyceryl alkyl esters are good foaming agents but the ester linker can be sensitive to pH, chemicals and temperature unlike the ether function. In this work, the foaming properties of a diglyceryl ether, namely 1-*O*-dodecyl diglyceryl ether ($C_{12}Gly_2$), are compared to those of *n*-dodecyl-β-D-maltoside ($C_{12}Glc_2$) and pentaethyleneglycol monododecyl ether ($C_{12}E_5$). The self-aggregation behaviour of $C_{12}Gly_2$ and adsorption at the air-water interface has been first investigated. For the three surfactants, the dynamic response of the interface, measured in oscillatory bubble interfacial rheology experiments below CMC, is compared and put in relation with their foaming properties. In particular, the foamability by air sparging at a concentration of 10 times the CMC, the foam stability over 1h and the foam density are quantified.

It is shown that $C_{12}Gly_2$ forms liquid crystals at low concentration (~10 CMC). $C_{12}E_5$, with a lower elasticity high frequency limit ε_0, forms unstable foam with quick drainage and

breakdown, whereas higher ε_0 surfactants $C_{12}Gly_2$ and $C_{12}Glc_2$ form much more stable foams, resulting from hydrogen bonds between the polar heads of $C_{12}Glc_2$ and $C_{12}Gly_2$. Differences in $C_{12}Gly_2$ and $C_{12}Glc_2$ foams lay in initial bubble size (smaller for the $C_{12}Glc_2$). In $C_{12}Gly_2$ foam, the main destabilization phenomenon is coalescence over drainage, and the foam volume only decreases by 30% in 1 hour.

Keywords: 1-O-dodecyl diglyceryl ether, foam, dilational surface rheology, foam stability, non-ionic surfactants.

1. Introduction

Foams, consisting of gas bubbles dispersed and stabilized in a liquid or solid matrix, are found in a variety of end-use products including construction materials, toiletries, but also food and beverages. In an aqueous matrix, foam generation requires stabilizing the gas/water interface, usually by means of surface-active molecules, so as to achieve good foamability and foam stability.

It was shown that foamability of a surfactant solution is greatly influenced by the nature and surface properties of the surfactant. Indeed, correlation between dynamic surface tension and foamability was reported,[1–4] and the faster the surfactant adsorbs at the interface, the higher the foamability is.[5] Also, it directly depends on the critical micelle concentration (CMC) as lower CMC corresponds to higher foamability.[6]

On the other hand, foam stability is a measure of a foam's lifetime. Three main phenomena contribute to destabilize foams, namely liquid drainage, Ostwald ripening, and bubble coalescence.[1,7,8] Slowing down or limiting those processes allows improving foam stability. First of all, it was shown that drainage can be limited by increasing the solution viscosity or the surface elasticity and viscosity.[1] Ostwald ripening is favored by large bubble size dispersity and solubility of the gas in the solution, and is thus reduced in monodisperse foams and by reducing the gas permeability through the surface surfactant layer. This is thought to be linked with surface viscoelastic properties.[9] Tcholakova et al. showed that high elastic modulus of the adsorbed surfactant layer contributes to reducing the Ostwald ripening rate in surfactant stabilized foams.[10] Finally, coalescence can be stemmed by increasing the film resistance to rupture, which is believed to depend on the surface viscoelasticity.[2,11,12] In other words, surface viscoelastic properties are involved in all three foam destabilization phenomena, and are thus of first importance in foam studies.

Dispersed liquid crystal (LC) phases have been shown to stabilize both aqueous and non-aqueous foams.[13–17] Indeed, the presence of dispersed Lα lamellar liquid crystals increases the film viscosity, thus leading to a decrease of the liquid drainage. Moreover, their

contribution to foam stabilization can be attributed to the covering of bubbles by the particles, reducing gas diffusion. Finally, they prevent bubble coalescence by avoiding bubble collision.[16]

In this work, we report the foaming properties of the 1-*O*-dodecyl diglyceryl ether ($C_{12}Gly_2$) surfactant, synthesized in the laboratory so as to study the pure regioisomer. Shi et al.[18] described a green catalytic reductive etherification of diglycerol with linear aldehydes to produce a mixture of 1-*O*-alkyl and 2-*O*-alkyl diglyceryl ethers (selectivity > 9/1). Sagitani et al. showed the ability of $C_{12}Gly_2$ to form LC phases in aqueous solution.[19] Similar surfactants such as diglycerol fatty acid esters are able to form LC at low concentration,[20] and were reported by Shrestha et al. as good foam stabilizers.[16] $C_{12}Gly_2$ has been reported as an effective solubilizing agent forming Winsor III microemulsions at low concentration and as a promising emulsifying agent [19,21] but to our knowledge, its foaming properties have never been described.

Among other nonionic surfactants, such as polyethoxylated fatty alcohols (C_iE_j) and alkylpolyglucosides (C_nGlc_m), the strength of H-bonds was found to be of importance regarding foaming properties,[22] attributed to the influence on surface viscoelasticity. Indeed, Stubenrauch et al.[23] showed the importance of intermolecular H-bonds in foam stabilization for a various C_{12}-chain surfactants bearing different types of polar heads. Surfactants bearing oligo(ethylene oxide),[22,24–26] phosphine oxide,[27,28] trimethyl ammonium,[27,28] sarcosinate,[29] amine oxide at pH ≠ 5,[30] or carboxylic acid at pH ≠ pKa[31] as polar head produce foams that are not very stable. On the contrary, surfactants bearing a sugar-type polar head are good foam stabilizers.[22,24,25,30]

Those results point out the importance of intermolecular interactions in foam stabilization. We discuss the properties of aqueous solutions and foams stabilized by C_{12}-chain nonionic surfactants, the $C_{12}Gly_2$ in comparison with *n*-dodecyl-β-D-maltoside ($C_{12}Glc_2$) and pentaethylene glycol monododecyl ether ($C_{12}E_5$), differing by the nature of their polar head as shown in Figure 1, and their lyotropic behaviour.

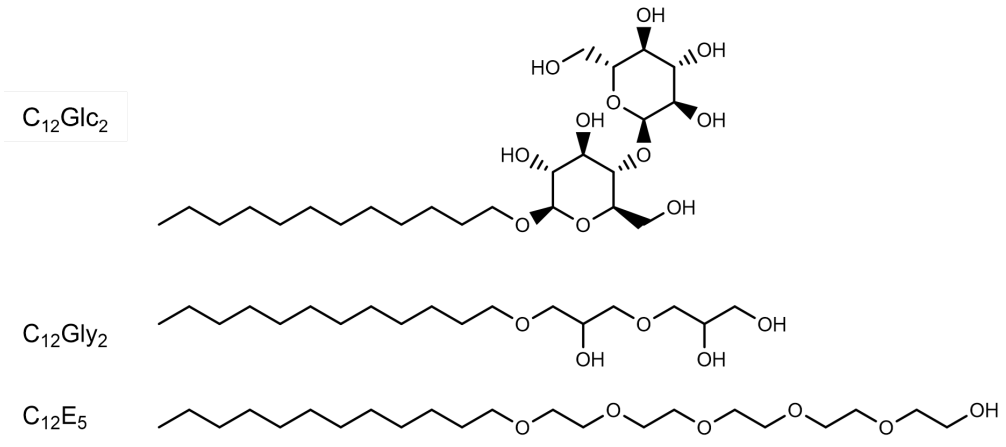

Figure 1. Molecular structures of *n*-dodecyl-β-D-maltoside ($C_{12}Glc_2$), 1-*O*-dodecyl diglyceryl ether ($C_{12}Gly_2$) and pentaethylene glycol monododecyl ether ($C_{12}E_5$) studied in this work.

$C_{12}E_5$ was chosen because its hydrophilicity quantified by the HLB value is the closest (11.7, calculated using Griffin's equation)[32] to the $C_{12}Gly_2$ (11.6, calculated by the PIT-slope method).[33] $C_{12}Glc_2$ was chosen as a reference surfactant because its foaming and surface rheological properties are well described in the literature.[11,12,22,24,26,34,35] Its hydrophilicity according to the HLB is 14.4,[36] clearly higher than $C_{12}Gly_2$ and $C_{12}E_5$. Firstly, the self-aggregation behaviour in dilute solution and the behaviour of binary water/surfactant mixtures at higher concentration are investigated. Secondly, dilational surface rheology for $C_{12}Gly_2$ and $C_{12}E_5$ are performed and compared with reported data for $C_{12}Glc_2$.[37] Finally, foamability and foam stability results are discussed in terms of surface tension data as well as on dilational surface elasticities and interpreted based on the differences of the nature for the three types of polar heads and lyotropic behaviour of surfactants.

2. Materials and methods

2.1. Chemicals

Pentaethylene glycol monododecyl ether ($C_{12}E_5$, > 98.0%) was purchased from TCI chemicals and *n*-Dodecyl *β*-D-maltoside ($C_{12}Glc_2$, > 98.0%) was purchased from Sigma Aldrich. 1-*O*-dodecyl diglyceryl ether ($C_{12}Gly_2$) was synthesized in the lab according to the following procedure.

Selective synthesis of 1-O-dodecyl diglyceryl ether ($C_{12}Gly_2$) (Scheme 1). $ZnCl_2$ (8.9 g, 0.065 mol, 0.06 eq.) was dissolved under stirring in 1-dodecanol (200.5 g, 1.078 mol, 1 eq.) and heated to 100 °C. Epichlorohydrin (109.2 g, 1.180 mol, 1.1 eq.) was added dropwise for 4 h. After cooling to 50 °C, $NaOH_{aq}$ 50% (86.2 g, 1.078 mol, 1 eq.) was added dropwise for 1 h. The mixture was kept under stirring at 50 °C for 4 h. After cooling to R.T., the mixture was washed with 3x120 mL of water to remove salts. The crude was dried over $MgSO_4$, filtered and distilled under vacuum pressure (7×10^{-2} mbar) between 134 and 138 °C to yield 65.2 g of a mixture of dodecyl glycidyl ether (82% GC-FID) and dodecylchlorhydrin ether (18% GC-FID). This mixture was added dropwise for 1 h to a solution of sodium solketalate prepared previously by dissolving Na(s) plates (7.4 g, 0.322 mol, 1.2 eq.) in solketal (177.0 g,1.339 mol, 5 eq.) at R.T. for 4 h then 60 °C for 20 h under N_2 flow. The mixture was stirred at 50 °C for 20 h, cooled to R.T., dissolved in 100 mL diethyl ether and washed with 3x100 mL water. The organic phase was dried over $MgSO_4$, filtered and solvent was evaporated. The crude was distilled under vacuum pressure (4×10^{-2} mbar) between 160 and 165 °C to yield a colourless liquid (80.2 g, 96% GC-FID, two-steps yield = 82%). The product (35.9 g, 0.096 mol) was diluted in 120 mL methanol, trifluoroacetic acid (TFA, 1.2 mL, 0.016 mol, 1.8 g) was added and the mixture was stirred at R.T. for 96 h. The reaction was

monitored by ^{1}H NMR. Once the reaction was complete, solvent and TFA were removed by rotative evaporation, yielding 1-*O*-dodecyl diglyceryl ether as a white powder (31.5 g, > 98% (^{1}H NMR), yield = 98%).

^{1}H NMR (300 MHz, DMSO-d_6) δ 4.55 (s broad, 3H), 3.68 (quint *a*, *J* = 5.5 Hz, 1H), 3.56 (quint *a*, *J* = 5.6 Hz, 1H), 3.44 – 3.22 (m, 10H), 1.46 (q, *J* = 6.6 Hz, 2H), 1.24 (s, 18H), 0.84 (t, *J* = 6.5 Hz, 3H).

^{13}C NMR (75 MHz, DMSO-d_6) δ 72.88, 72.13, 70.50, 70.42, 68.50, 68.48, 63.01, 31.25, 29.15, 29.01, 28.98, 28.85, 28.67, 25.59, 22.05, 13.88.

^{1}H and ^{13}C NMR spectra are available in the Supporting Information.

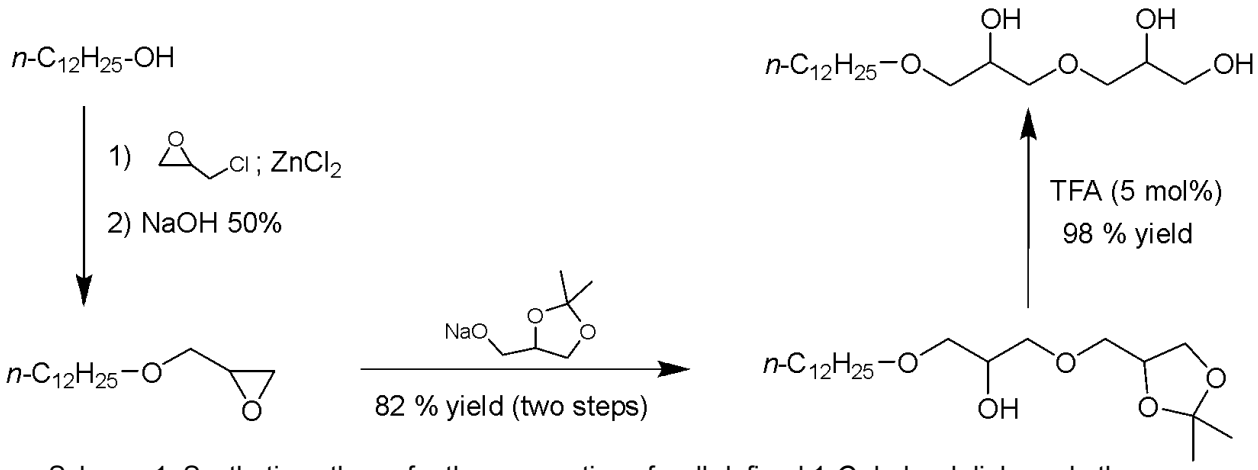

Scheme 1. Synthetic pathway for the preparation of well-defined 1-*O*-dodecyl diglyceryl ether.

2.2. Surface tension measurement and CMC determination

Critical micellar concentration (CMC) determination by surface tension measurements was carried out with a Krüss K100 tensiometer (Krüss GmbH, Germany) using a Du Nouy ring. Surface tension before CMC was fitted by Langmuir-Szyszkowski equation of state given in equation (1). This model been widely applied to adsorbed surfactants, and was shown to describe well the dependence of the surface tension γ with the surfactant concentration for low molecular surfactants.[11,38] This model considers no interactions between adsorbed molecules.

$$\gamma = \gamma_0 - RT\Gamma_\infty \ln ln\left(1 + \frac{c}{a}\right) \quad (1)$$

In this equation, γ (mN.m^{-1}) is the measured surface tension, γ_0 is pure water surface tension, i.e. 72.0 mN.m^{-1}, R (mol^{-1}. K^{-1}) is the gas constant, T (K) is the temperature, i.e. 298 K, Γ_∞ (mol.m^{-2}) is the maximum surfactant surface concentration, c (mol.L^{-1}) is the bulk surfactant

concentration and a (mol.L^{-1}) is the bulk concentration for which $\Gamma = \frac{\Gamma_\infty}{2}$. The area per molecule A_m (m^2) can then be calculated as follows.

$$A_m = \frac{1}{N_A \Gamma_\infty} \quad (2)$$

where N_A (mol^{-1}) is the Avogadro number.

2.3. Microscopy and Dynamic Light Scattering

Aqueous systems were observed at the optical microscope (Keyens VHX-900 F) equipped with cross polarizers. Particle-size measurements were performed using a Zetasizer Nano ZS (Malvern). Light-scattering cells of 10 mm were used. All measurements were performed at 173°. The time-correlation function of the scattered intensity allows calculating a hydrodynamic radius of the droplet using the Stokes–Einstein equation. The data are analyzed by cumulative analysis to obtain an average diffusion coefficient and subsequently by CONTIN analysis in order to obtain information about the entire distribution of the particle size. Solutions were prepared by dissolving the surfactant in water and then agitating 30 min at ultrasonic bath Bandelin (Sonorex Digitec). In order to study the influence of agitation on the size of aggregates two other protocols were studied for the 5×10^{-4} M $C_{12}Gly_2$ solution. First, magnetic stirring at 750 rpm for 1h30 and then this sample was agitated again using an ultrasonic probe Sonotrode S26d2 (2 mm diameter) immersed by 5 mm in the liquid and operated by the ultrasonic processor UP200St (both from Hielscher) for 1m30s. The sonotrode pulse was fixed at 100% and the amplitude at 80%. To study the change in temperature by DLS, the samples prepared at 25°C were heated until 40°C and then the temperature in DLS was also fixed at this value.

2.4. Dilational interfacial rheology

The surface dilational rheological properties of surfactant solutions were studied at 25 °C using a TRACKER™ automatic drop tensiometer (Teclis Instruments, France). Solutions at concentrations from 0.1, 0.5 and 1 CMC were studied for $C_{12}E_5$ and $C_{12}Gly_2$. A bubble of 5 µL was formed at the tip of a needle connected to a syringe in the rising drop configuration and left to rest until the interface was stabilized: the surface tension stabilization isotherm was monitored by image analysis of the contact angle between the needle and the bubble. In this work, 1 h equilibration was sufficient. At the end of this period, 10 sinusoidal oscillations of amplitude 0.8 µL were imposed to the bubble by oscillation of the motor-driven syringe plunger. The experiment was repeated within the accessible frequency range of oscillation (10^{-2} Hz to 1 Hz), causing sinusoidal changes in the surface area and the drop shape. The changes in drop shape were monitored by a video camera, and the corresponding changes in surface tension were calculated using the TRACKER™ 2020 software. Surface tension

variation with bubble area over time was processed to calculate the surface dilational visco-elasticity E ($mN.m^{-1}$) according to equation (3).

$$E = \frac{d\gamma}{d\ln ln\, A} \tag{3}$$

where γ ($mN.m^{-1}$) is the bubble surface tension and A (m^2) is the bubble area. The surface dilational visco-elasticity E is a complex function of the perturbation frequency ν, whose real part ε_r is the dilational elasticity and the imaginary part ε_i is related to the dilational viscosity η ($s.mN.m^{-1}$) as given in equation (4).

$$E = \varepsilon_r + i\varepsilon_i = \varepsilon_r + 2\pi\nu i\eta \tag{4}$$

In this expression, $2\pi\nu = \omega$ is the oscillation pulse ($rad.s^{-1}$).

The dilational viscoelasticity has been related to thermodynamic parameters by theorical equations like the Lucassen-Van den Tempel model.[39,40] This model considers “a diffusion-controlled adsorption system”, in which there is no barriers to adsorption/desorption in the interface and the increase of adsorption is equal to the diffusion. The experimental E is a function of the high frequency limit of dilational surface elasticity ε_0, see equation (5), and the dephasing angle φ (rad) between area deformation and surface tension variations, see equation (6).

$$|E| = \frac{\varepsilon_0}{\sqrt{1+2\xi+2\xi^2}} \tag{5}$$

$$\tan tan\, \varphi = \frac{\xi}{1+\xi} \tag{6}$$

$$\text{with } \xi = \sqrt{\frac{\omega_0}{4\pi\nu}} \tag{7}$$

where ω_0 is the molecular exchange parameter and ν the frequency. The ε_0 and ξ parameters are related to the thermodynamic behaviour and the transport properties of the surfactant by the $\frac{d\gamma}{dln\Gamma}$ and the diffusion coefficient “D” of the surfactant at the bulk, respectively. Using equations (5) and (6), one obtains the expression of ε_0 independent of the frequency as given in equation (8).The same way, ω_0 can be written independently of the frequency as stated in equation (9).[37]

$$\varepsilon_0 = \frac{|E|}{\cos cos\, \varphi - \sin sin\, \varphi} \tag{8}$$

$$\omega_0 = 4\pi\nu \frac{tg^2\varphi}{(1-tg\varphi)^2} \tag{9}$$

ε_0 and ω_0 were calculated at each frequency for $C_{12}E_5$ and $C_{12}Gly_2$ surfactants solutions, averaged and compared to the fitted values in the Supplementary Information. The evolution with the oscillation frequency of ε_r and η was modelled with equations (10) and (11) respectively.[37]

$$\varepsilon_r = \varepsilon_0 \frac{1+\xi}{1+2\xi+2\xi^2} \quad (10)$$

$$\eta = \frac{\varepsilon_0}{2\pi\nu} \frac{\xi}{1+2\xi+2\xi^2} \quad (11)$$

2.5. Foaming capacity and stability

Dynamic foam stability experiments were conducted using a Krüss Dynamic Foam Analyzer DFA 100 (Krüss GmbH, Germany). Foam was generated in a glass column of height 250 mm and diameter 40 mm by air sparging through a porous paper filter (pore size 12-15 µm) in 50 mL of surfactant solution at a flow rate of 0.2 L/min until a total height of 180 mm was reached. An optical camera, fixed at a height of 10 cm, monitored the foam evolution (number and volume of bubbles on a certain area) for 60 min. The volume of both foam and solution was monitored over time, and the liquid fraction in the foam part f_{liq} was calculated as follows.

$$f_{liq}(t) = \frac{V_{i,sol} - V_{sol}(t)}{V_{foam}(t)} \quad (12)$$

with $V_{sol}(t)$ and $V_{foam}(t)$ the solution and foam volumes (mL) respectively, and $V_{i,sol}$ the initial solution volume before foam generation by air sparging. All experiments were done at least in triplicate.

3. Aggregation behaviour in aqueous solution and surface activity

The binary $C_{12}Gly_2$/water mixtures were shown to form LC in equilibrium with aqueous solution up to a concentration of 55 wt.%. Beyond this concentration, lamellar L_α phase is formed.[19] In this work, closer attention was brought to the behaviour of dilute solutions, in particular so as to approach the solubility limit of $C_{12}Gly_2$. Between 1×10^{-4} and 3×10^{-4} M (0.003-0.010%) there is an increase in aggregate size measured by DLS and shown in Figure 2a. Observations with a polarized optical microscope confirmed the presence of LC phases (Figure 2b and 2c) and probably the presence of vesicle structures (Figure 2c). Those vesicles could be formed from bilayers similar to the lamellar phase and are not thermodynamically stable. Indeed, changing the agitation protocol to prepare the solutions in Figure 2a modifies drastically the size of aggregates (see Figure S4A in Supporting Information). If just magnetic stirring is applied to the 1×10^{-3} M sample, the size is near 190nm and after 1m30s of ultrasounds using a sonotrode the size decreases until 19 nm.

No change was observed in the structures over a temperature range of 25°C to 60°C for the 1.5×10^{-2} M solution prepared using ultrasonic bath (see Figure S5 in Supporting Information). However, the temperature has an important influence in the size distribution when the sample is prepared with magnetic stirring and in this case an increase of temperature until 40°C diminishes notably the average size (see Figure S4B in Supporting Information).

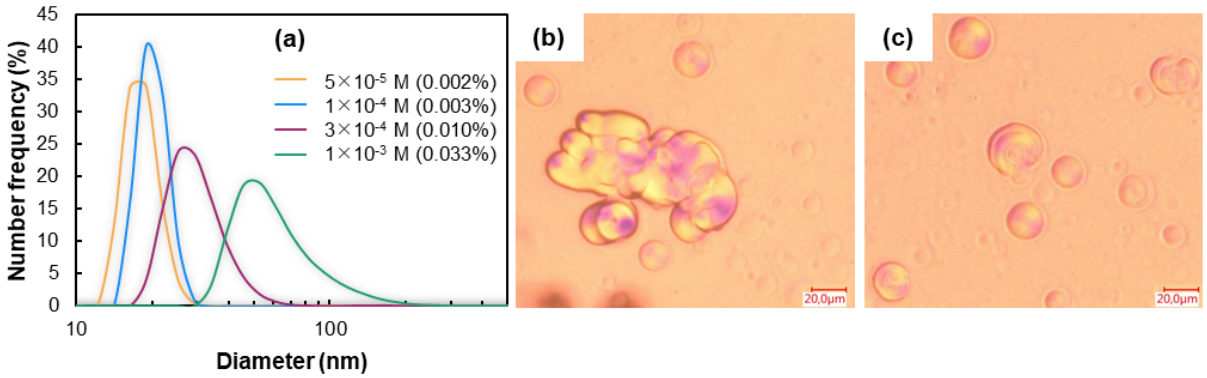

Figure 2. (a) Aggregate size distribution in $C_{12}Gly_2$ solutions measured by DLS at 25.0 °C. Up to 1×10^{-4} M (0.003 wt.%), aggregate size corresponds to presumed micelle structures. From 3×10^{-4} M (0.010 wt.%), bigger objects are formed. (b) Photo from optical microscope with polarized light for a 1.5×10^{-2} M solution (0.502 wt.%) shows LC in equilibrium with aqueous solution and probably vesicle structures (c).

The formation of LC phases is common with nonionic surfactants, especially for the series of polyethoxylated alcohols C_iE_j.[41] Below the cloud point, $C_{12}E_5$/water system forms an isotropic solution L_1 at 25°C until a concentration of about 45 wt.% at which a hexagonal phase H_1 is obtained. L_α phase is formed at higher concentrations.[42] Regarding sugar-based surfactants, $C_{12}Glc_2$/water systems form isotropic solutions up to 45 wt.% and L_α phase at higher concentrations.[43] In both cases, dilute samples are isotropic solutions at room temperature. The formation of LC phases is related to interactions among polar heads, water molecules and hydrophobic chains.[44] The fact that LC form at low concentration in $C_{12}Gly_2$/water mixtures is indicative of preferential intersurfactant interactions over surfactant-water interactions, which is not the case for $C_{12}Glc_2$ and $C_{12}E_5$. Interestingly, a similar phase behaviour to that of $C_{12}Gly_2$, i.e. LC formation in equilibrium with aqueous solution at concentrations as low as 2 wt.% and vesicle formation, was reported in the case of diglycerol monolaurate, which only structural difference from $C_{12}Gly_2$ is an ester link instead of an ether one.[20] Other oligoglycerol esters were shown to form L_α phase dispersions at low concentrations.[20,45]

The behaviour of $C_{12}Gly_2$ aqueous solutions at much more dilute concentrations allowed the determination of its critical micelle concentration (CMC), compared to that measured by

Sagitani et al.[19] Both isotherms are shown on Figure 3 and were fitted with a Langmuir-Szyszkowski model.

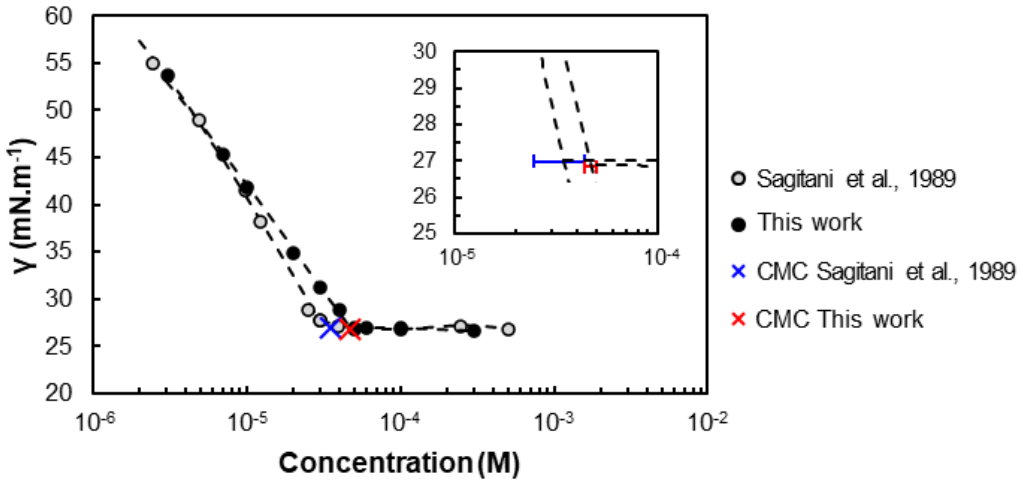

Figure 3. Surface tension isotherm of $C_{12}Gly_2$ at 25.0 °C compared to that of Sagitani et al.[19] Data before CMC is fitted with a Langmuir-Szyszkowski model as given in equation (1). Error bars are indicated in the zoom. Blue for the data of Sagitani et al. [19] and red for our data.

Minimal surface tension γ_{min} = 26.8 mN.m^{-1} agrees well with the value of 27.0 mN.m^{-1} determined by Sagitani et al.[19] Compared with $C_{12}E_5$ and $C_{12}Glc_2$, $C_{12}Gly_2$ causes the greatest decrease in surface tension since γ_{min} = 30.5 mN.m^{-1} for $C_{12}E_5$[46] and γ_{min} = 36.4 mN.m^{-1} for C_{12} Glc_2.[47] The CMC for $C_{12}Gly_2$ obtained here (4.7×10^{-5} M) and in the literature (3.5×10^{-5} M) are very close as can be seen in Figure 4. In comparison with the two other surfactants under study, the CMC value of $C_{12}Gly_2$ is comparable to that of $C_{12}E_5$ (6.4× 10^{-5} M)[46] but inferior by an order of magnitude to that of $C_{12}Glc_2$ (1.5×10^{-4} M)[48], which has greater molecular solubility in water, potentially due to more hydrophilic polar head forming strong interactions with water molecules. Compared to the homologous ester, the CMC value is slightly inferior to that of diglyceryl monolaurate (1×10^{-4} M), probably due to the reduced hydrophilicity and thus aqueous solubility of the ether bond *vs* the ester one. Minimal surface tensions are comparable (γ_{min} = 27.7 mN.m^{-1} for diglyceryl monolaurate).[49]

Parameters of the Langmuir-Szyszkowski model and the resulting area per molecule A_m are presented in Table 1. The area per $C_{12}Gly_2$ molecule is larger in this work, meaning that the interface is less densely packed compared to the results of Sagitani et al., but differences in fitting parameters are small and a and Γ_∞ values are of the same order of magnitude. Further interpretations will be based on values determined in this work.

Table 1. Fitting parameter of Langmuir-Szyszkowski equation for $C_{12}Gly_2$ and associated area per molecule A_m calculated from equation (2). Γ_∞ and A values are compared to those of $C_{12}Glc_2$ and $C_{12}E_5$ from literature data.

	a (M)	Γ_∞ (mol·m^{-2})	A_m (Å^2)
$C_{12}Gly_2$ (This work)	5.35×10^{-7}	4.1×10^{-6}	41
$C_{12}Gly_2$ [19]	8.95×10^{-7}	5.1×10^{-6}	33
$C_{12}Glc_2$ [11]	4.59×10^{-6}	4.5×10^{-6}	37
$C_{12}E_5$ **[46]**		3.3×10^{-6}	50

Surprisingly, the most densely packed interface is the one covered with $C_{12}Glc_2$ with the smallest area per molecule, yet the maltoside polar head is the largest of the three surfactants under study. This is indicative of important intermolecular interactions. The area per $C_{12}Gly_2$ molecule is close to that of $C_{12}Glc_2$. In contrast, $C_{12}E_5$ forms the least dense surface film, probably due to weaker interactions between the hydrophilic heads E_5, compared to the intermolecular interactions of Gly_2 and Glc_2 forming a greater number of hydrogen bonds. Frumkin and Henry models were also used to fitting the surface tension data before the CMC and results are very close to those obtained with Langmuir-Szyszkowski model (see figure S3 and Table S1 in Supporting information). The β value of the Frumkin equation is slightly positive, indicating attractive interactions as expected.

4. Dilational surface rheology

The surface rheological properties of $C_{12}Gly_2$ and $C_{12}E_5$ solutions were determined by varying the oscillation frequency at different concentrations (0.1, 0.5 and 1 CMC). Data were extracted from literature for $C_{12}Glc_2$ for comparison purposes.[37] Typical examples of surface tension response to bubble volume sinusoidal oscillations at 0.25 Hz are presented in Figure 4 in the case of 0.1 CMC and 1 CMC $C_{12}Gly_2$ solutions. The response of both solutions to the variations in the surface area of the droplet is different in terms of both the surface tension amplitude and the angle phase between both curves. At 0.25 Hz, the amplitude in the surface tension is bigger (10 vs. 7 mN/m) for the more diluted solution. Comparing the surface tension and the bubble area profiles, the angle φ is bigger for the solution at the CMC. The gap between the surface tension and bubble area curves is more pronounced and the angle must be larger for the solution at the CMC.

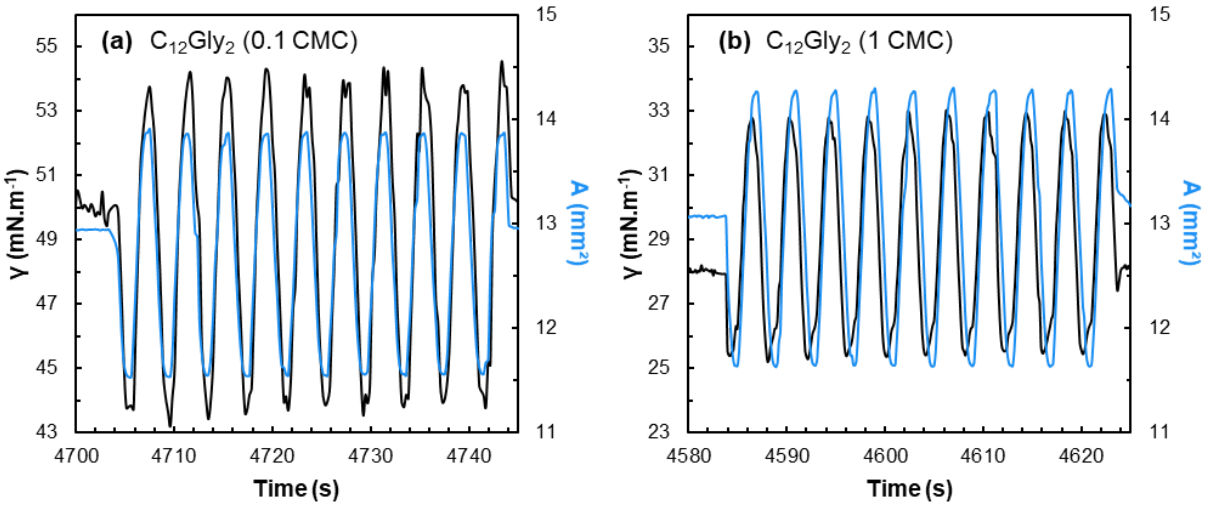

Figure 4. Surface tension (black) and surface area (blue) of oscillating bubbles at a frequency of 0.25 Hz for (a) 0.1 CMC and (b) 1 CMC solutions of $C_{12}Gly_2$.

Based on those measurements, the dephasing angle φ, surface elasticity ε_r and viscosity η are calculated by Fourier transformation as described in the experimental section. The evolution of ε_r and η as a function of the oscillating frequency are shown in Figure 5. Experimental data were fitted with the Lucassen-Van den Tempel model according to equations (10) and (11), ε_0 and ω_0 being fitting parameters.

Dilational surface elasticities ε_r show the same evolution with the increase in frequency for all surfactants. For the most diluted solutions (0.1 CMC), ε_r increases until reaching a plateau. This plateau, corresponding to ε_0, represents the high frequency limit of the dilational surface elasticity which values are given in Table 2. As the bulk concentration increases, so does the bubble surface covering and thus its elasticity at high frequencies. At the frequency range investigated in this work, the elasticity limit cannot be reached and the values in Table 2 for 0.5 CMC and at the CMC are less exacts than those for 0.1 CMC because they are the result of an extrapolation in which no points are in the vicinity of the plateau zone.

Accurate determination of ε_0 would require investigating the surface viscoelasticity at high frequencies. The elasticity limit is reached for $\nu > \frac{\omega_0}{2\pi}$. That is why the ε_0 plateau is reached only for the lowest concentrated solutions in Figure 5, as the range of frequency corresponds to the order of magnitude of ω_0. For higher concentrations than 0.5 CMC, $\frac{\omega_0}{2\pi} > \nu$ meaning that the surfactant surface layer cannot be considered insoluble and purely elastic as the exchanges processes between the bulk and the surface are non-negligible.[11,50] In the case of $C_{12}E_5$ at 1 CMC, the fitted ε_0 and ω_0 values are not consistent with the expected

evolution. ε_0 value at 1 Hz is barely 19 mN.m$^{-1,}$ which is too low compared to that at 0.5 CMC which is of 45 mN.m^{-1}, allowing the extrapolation of ε_0 limit. Instead, at 1 CMC, ε_0 and ω_0 were calculated at each frequency according to equations (8) and (9) and averaged to yield the values reported in Table 2. Comparison of values obtained by each method is given in Table S1 of the Supplementary Information. The reader should be aware that ε_0 and ω_0 values given in Table 2 must be considered cautiously and are only indicative of an order of magnitude as important differences were reported for similar surfactants in similar conditions.[37]

Elasticity limit values ε_0 at 1 CMC are such that $C_{12}Gly_2$ > $C_{12}Glc_2$ > $C_{12}E_5$. This trend is in accordance with the density of molecules adsorbed at the interface determined in this work. However, the order of evolution is inverted for the molecular exchange parameter ω_0 which is the highest for $C_{12}Glc_2$ and lowest for $C_{12}Gly_2$. High ω_0 indicates higher molecule mobility.

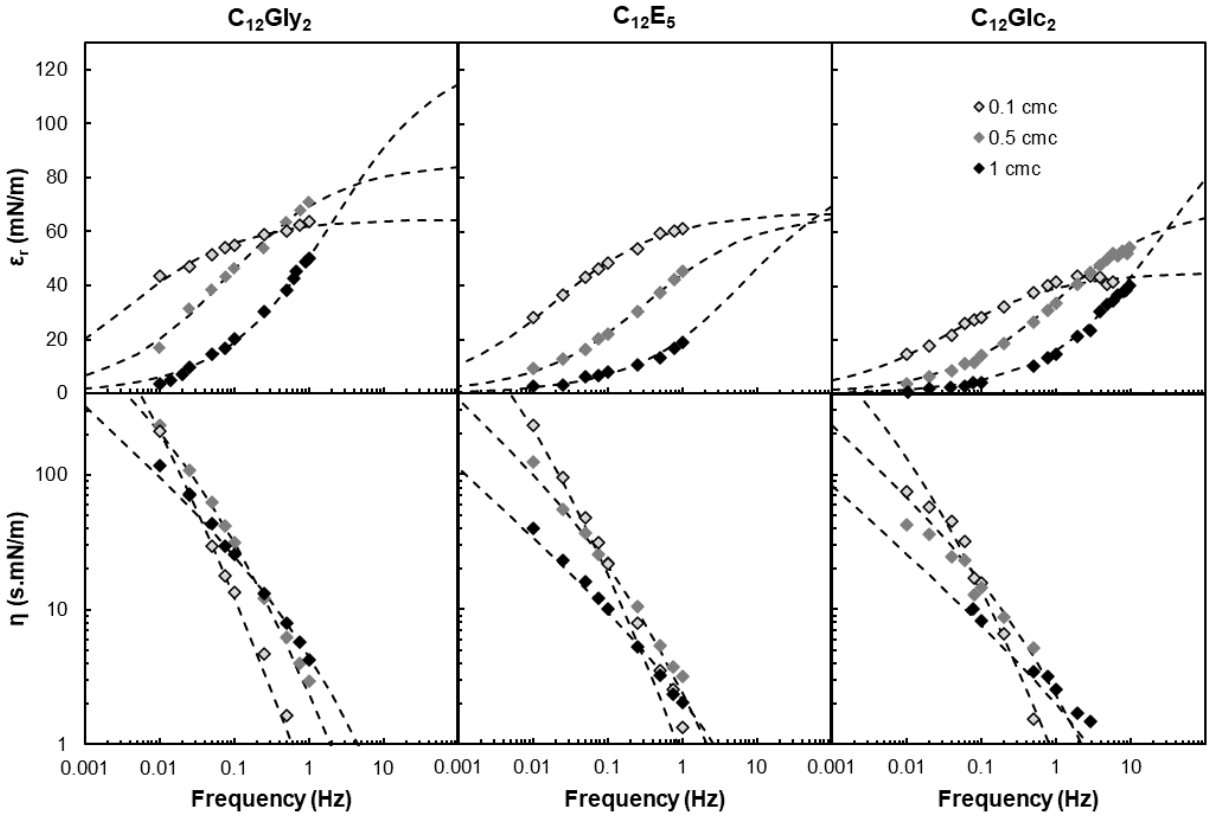

Figure 5. Dilational surface elasticity and viscosity of $C_{12}Gly_2$ (left, CMC = 4.7×10^{-5}M), $C_{12}E_5$ (center, CMC = 6.4×10^{-5} M)[46] and $C_{12}Glc_2$ (right, CMC = 1.5×10^{-4} M,[48] extracted and reproduced from Boos et al., 2013)[37] as a function of the oscillation frequency ν for concentrations of 0.1 CMC (◇), 0.5 CMC (◆) and 1 CMC (◆).

Surface viscosity η decreases inversely proportional to the frequency and Figure 5 shows the viscosity in logarithmic scale in order to better visualize the changes. In our case, at low frequencies, the viscosity seems decrease with higher concentrations of surfactant. At high

frequencies the values are equivalent. The evolution of both ε_r and η with increasing oscillation frequency reflects the resistance of surfactant molecules towards desorption, attributed to interaction strength between molecules inside the interfacial film.

Table 2. High frequency limit of dilational surface elasticity ε_0 (mN.m^{-1}) for $C_{12}Gly_2$, $C_{12}E_5$ and $C_{12}Glc_2$ (from Boos et al., 2013) [37] and molecular exchange parameter ω_0 (rad.s^{-1}) values for $C_{12}Gly_2$ and $C_{12}E_5$ at 0.1 CMC, 0.5 CMC and 1 CMC.

	0.1 CMC		0.5 CMC		1 CMC	
	ε_0 (mN.m^{-1})	ω_0 (rad.s^{-1})	ε_0 (mN.m^{-1})	ω_0 (rad.s^{-1})	ε_0 (mN.m^{-1})	ω_0 (rad.s^{-1})
$C_{12}Gly_2$	64.6 ± 1.2	0.024 ± 0.007	85.5 ± 1.4	0.49 ± 0.05	127.5 ± 6.2	12.8 ± 1.7
$C_{12}E_5$	67.3 ± 0.4	0.118 ± 0.005	67.3 ± 1.5	2.1 ± 0.2	84.6 ± 5.8	44.8 ± 10.8
$C_{12}Glc_2$ [37]	45.3 ± 2.7	0.261 ± 0.004[a]	70.3 ± 4.2	7.1 ± 0.5[a]	114.2 ± 6.9	156 ± 27[a]

[a] Calculated from the experimental data reported by Boos et al., 2013.

5. Foam density and stability

The first step of forming a foam is the trapping of air bubbles into the solutions, also called foamability. In this work, foaming properties are studied at a concentration of 10 CMC so that the surface concentration is sufficient to attain fast air/water interface covering. All three surfactant solutions studied showed the same foamability at the air flow rate under study (Q = 200 mL.min^{-1}), *i.e.* the target total height of 180 mm (≈ 218 mL) was attained after approximately the same duration of air injection: 46 ± 1, 48 ± 2 and 46 ± 1 s for $C_{12}Gly_2$, $C_{12}Glc_2$ and $C_{12}E_5$, respectively. These values match well with the theoretical time calculated with the flow rate and a mass balance in gas: 50.3 s, indicating that there is no partial foam collapse during the generation. The characteristics of the resulting foams and their stability are analysed based on Advance software provided by Krüss. Foam characteristics like the total volume, foam liquid fraction and the mean bubble radius evolution over time are depicted in Figure 6a-c. Some examples of foam pictures are shown in Figure 7 for the three surfactants under study.

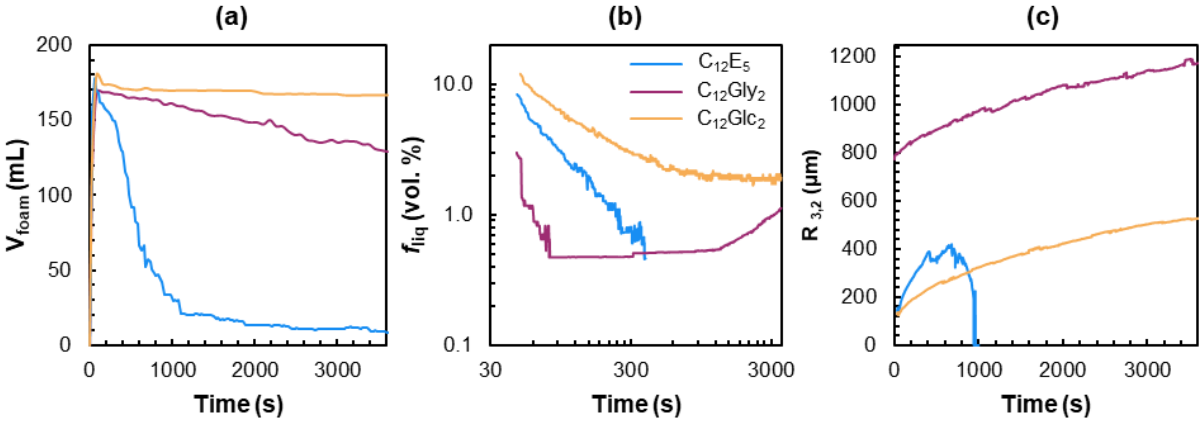

Figure 6. (a) Foam volume, (b) foam liquid fraction f_{liq} and (c) $R_{3,2}$ mean bubble radius evolution over time for $C_{12}Glc_2$, $C_{12}Gly_2$ and $C_{12}E_5$ 10 CMC solutions at 25.0°C. Foam is generated and analyzed using a Dynamic Foam analyzer DFA 100 (Krüss).

In the volume-time profile (Figure 6a), the behaviour of three surfactants is very different. As previously reported by Boos et al. using analogous foaming equipment,[25] $C_{12}Glc_2$ foam is very stable and dense with almost no V_{foam} decrease, highest stable fraction of liquid f_{liq} and the smallest bubbles over 1 hour. Even if the operating conditions are different (50 mL.min^{-1} N_2 and V_{foam} = 80 mL *vs*. 200 mL.min^{-1} Air and V_{total} = 180 mL) results in terms of stability are identical.

On the other hand, $C_{12}E_5$ forms the less stable foam with a total collapse after about 15 min (Figure 6a), a quick foam drainage in about 300 s (Figure 6b) causing bubbles to break until no more bubbles are detected by the camera as pointed out in the photo at t = 3000 s. Figure 7 also shows very large bubbles at 500 s. This result is also similar to the obtained profile for $C_{12}E_6$[25] in which V_{foam} decreases by 50% at only 140 s (460 s in our case). The behaviour of $C_{12}Gly_2$ in terms of the Volume-time profile is in between the $C_{12}Glc_2$ and the $C_{12}E_5$. However, the overall picture is not so trivial to interpret. Indeed, V_{foam} is maintained to over 70% of its initial value after 1 hour, but Figure 6b and c show that the foam is the less dense of all three with a low value of f_{liq} and the largest bubble size, but nevertheless stable over time. Those results are not intuitive as one would expect a foam with large bubbles and thin films to break up quickly.

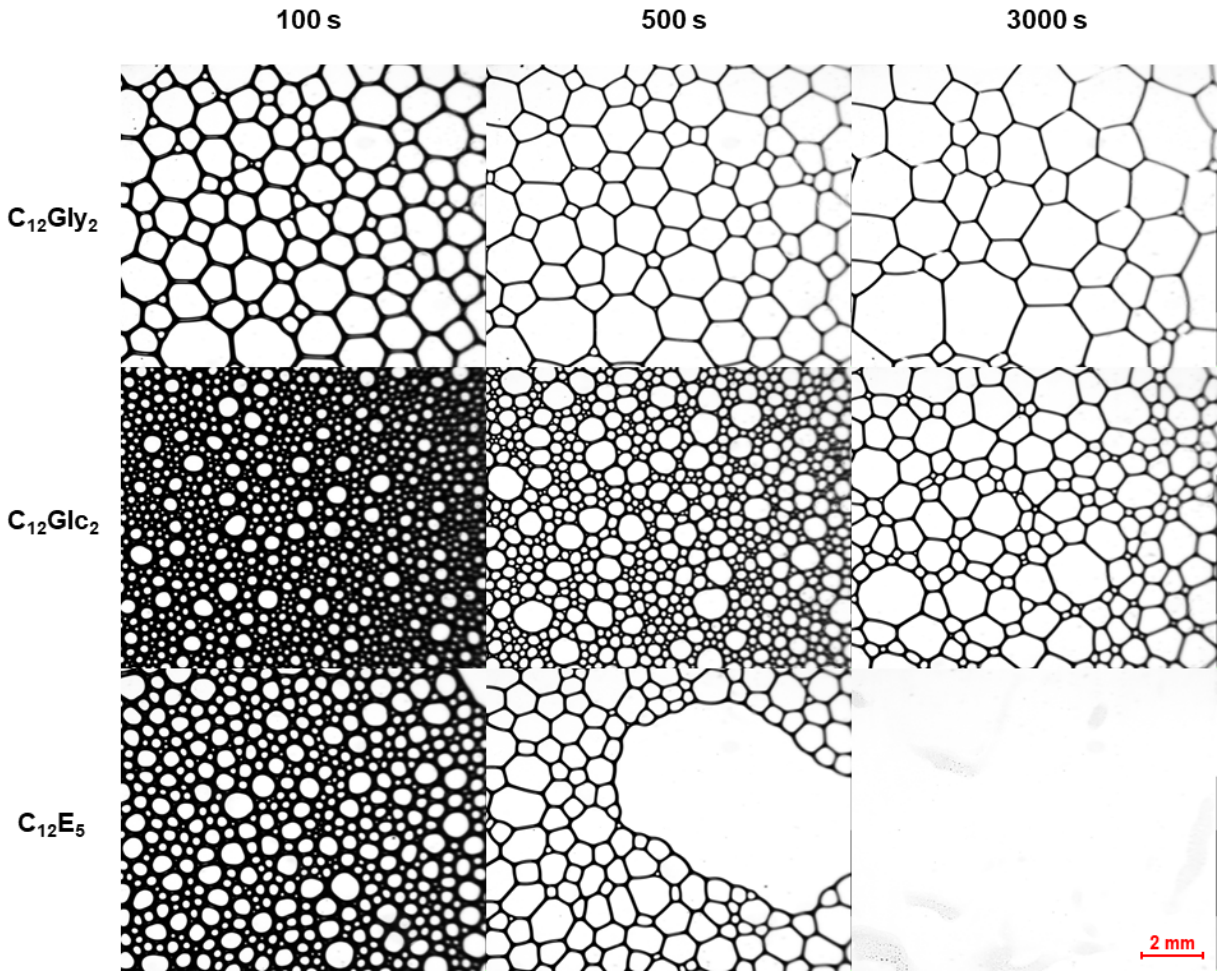

Figure 7. Original pictures of foam bubbles from DFA 100 data for $C_{12}Gly_2$ (top), $C_{12}Glc_2$ (middle) and $C_{12}E_5$ (bottom) solutions at 10 CMC, taken after 100 s (left), 500 s (centre) and 3000 s (right).

The bubbles created are the smallest for $C_{12}Glc_2$ ($R_{3,2}$=114±36 µm) and $C_{12}E_5$ (173±27 µm) and the largest ones are obtained with $C_{12}Gly_2$ solution (619±112 µm) as shown in Figure 6c and illustrated in Figure 7. The variation of the size with time are very similar for $C_{12}Glc_2$ and $C_{12}Gly_2$ even if their initial sizes are different. For $C_{12}E_5$, even if the initial size is similar to that of $C_{12}Glc_2$, the tendency is not constant. At the beginning the size increases faster than the other surfactants until reaching a critical collapse. At this point, the size seems to decrease because the number of analysed bubbles at the chosen height is insufficient and a value of 0 is finally obtained when no more bubbles are detected.

Film drainage governs the short-term foam stability, whereas coalescence governs the longer-term stability and coarsening, also known as Ostwald ripening, is not relevant.[25] It was shown that Ostwald ripening is controlled by the low frequency elasticity and coalescence by the high frequency elasticity ε_0,[51] and that for $\varepsilon_0 > \frac{\gamma}{2}$ Ostwald ripening is considerably slowed down.[52] Accordingly, gas permeability is reduced for high elastic modulus adsorbed layers, which is the case for all three surfactants.[10]

In the case of $C_{12}E_5$, the decrease in f_{liq} and the quick increase in $R_{3,2}$ coincide with quick V_{foam} decrease depicted in Figure 6a-c, indicating both drainage and coalescence. The observed coalescence rate is the most important for $C_{12}E_5$, for which ε_0 at 1 CMC is the smallest of the three surfactants under study. On the other hand, the $C_{12}Glc_2$ foam is slowly drained and coalescence is the main destabilization phenomenon. Even if foam structure evolves, volume is maintained. Finally, the behaviour of $C_{12}Gly_2$ foam is very different from the two others. It is the driest foam of all three with the smallest initial f_{liq} and quickest drainage. However, this does not seem to have any impact on foam stability given that the V_{foam} decrease rate is constant over 1 hour and there is no change in V_{foam} evolution even after the f_{liq} reaches its minimal value. In that case, destabilization can be attributed to bubble coalescence only. It results that elasticity limit at high frequencies ε_0 can be regarded as a relevant indicator of foam stability but results should be interpreted cautiously. Indeed, based on the hypothesis that thermally induced thickness and concentration fluctuations are responsible for foam film rupture, the high oscillation frequency range (200-800 Hz) should be of relevance in dilational rheology experiments, which would require other equipment.[53–55]

Coalescence rates are similar in $C_{12}Gly_2$ and $C_{12}Glc_2$ foams with an increase of about +400 µm in $R_{3,2}$ as their ε_0 values at 1 CMC are comparable (127.5 *vs*. 114.2 $mN.m^{-1}$). The faster V_{foam} decrease in $C_{12}Gly_2$ foam may thus be due to the initial larger bubble size. That way, one bubble rupture in the $C_{12}Gly_2$ foam has more impact on the global V_{foam} than one bubble rupture in the $C_{12}Glc_2$ foam. The formation of bubbles by air sparging is believed to be linked with the diffusion of surfactants to the newly created interface.[1] The molecular exchange parameter, ω_0, is one relevant parameter to rationalize this phenomenon: the lowest ω_0 value is obtained for $C_{12}Gly_2$, indicating slow exchanges between bulk and interface. ω_0 increases for $C_{12}E_5$, then again for $C_{12}Glc_2$, in accordance with the trend observed in bubble initial size. Diffusion phenomena are, however, irrelevant regarding foam stability as liquid drainage was shown to be faster than molecular diffusion.[56]

Several studies have shown that intermolecular H bonds have a major impact on foam stability by increasing the viscoelasticity of the surfactant film.[22–25,30,57,58] Strong H-bonds are formed between hydroxyl groups as they can act as both H-bond acceptors and donors, while ether groups only act as H-bond acceptors. The maltoside polar head bears the greatest number of hydroxyl groups (7) and forms about 5 intermolecular H-bonds and 5

H-bonds with water.[57] The diglycerol polar head in $C_{12}Gly_2$ bears 3 hydroxyls and 2 ether groups, reducing potential interactions compared to a maltoside. However, the low solubility of $C_{12}Gly_2$ points out its poor affinity for water, thus promoting intersurfactant interactions and potentially being responsible for quick foam drainage as shown in Figure 6b. No data were reported yet as to the number of H-bonds formed between chains. Finally, $C_{12}E_5$ only bears 1 hydroxyl and 5 ether groups, in accordance with the fact that the interface presents the largest area per molecule, the smallest surface elasticity limit and the poorest foam stability. Similar behaviour has been reported for $C_{12}E_6$.[37]

One interesting point regarding the behaviour of $C_{12}Gly_2$ stabilized foam is the formation of dispersed LC as described by Sagitani et al.[19] and developed in section 3 of this work. At a concentration of 10 CMC (4.7×10^{-4} M), the formation of LC contributes to reducing the effective molecular bulk concentration available for stabilizing the interface. On the other hand, as developed in the introduction, dispersed LC formed by diglycerol and oligoglycerol monoesters forming stable foams were shown to contribute to film stability by increasing the film visco-elasticity and adsorbing to the interface, thus reducing its permeability to gas.[13–17] The contribution of LC to visco-elasticity cannot be observed in dilational rheology experiments, given that LC are formed above the CMC and the diffusion-controlled hypothesis would not be verified. As expected, optical microscopic observations did not allow us to observe visible structures in the bubbles as those presented in figure 2b or 2c (at much higher concentrations) but the possibility of nanoaggregates stabilizing the interface should not be rule out. Some specific methods like confocal laser scanning microscopy could be used at several concentrations to verify this hypothesis.

6. Conclusions

Aggregation behaviour in water/$C_{12}Gly_2$ binary systems revealed the formation of vesicles, which are metastable structures, in dilute solutions from concentrations as low as ~10 CMC, and dispersed lamellar LC phase in equilibrium with aqueous solution. The spontaneous formation of vesicles in the dilute region points out the applicability of $C_{12}Gly_2$ in fields like drug delivery where vesicles are desired. The contribution of LC to surface elasticity could not be observed due to necessity of measuring viscoelastic properties in diffusion-controlled conditions, i.e., at $c \leq$ CMC. However, the contribution of LC dispersion to foam stabilization has been already shown in diglycerol monoesters, which present very similar structures to the surfactant under study.[16]

The CMC values and minimal surface tension were determined for $C_{12}Gly_2$ and compared to those of the polyethoxylated fatty alcohol ($C_{12}E_5$) and maltoside ($C_{12}Glc_2$) homologous. The $C_{12}Gly_2$ surfactant, previously reported as an effective solubilizing agent [19], or emulsifying

agent [21] was investigated here as a foam stabilizer and compared with $C_{12}E_5$ and $C_{12}Glc_2$. CMC were not correlated to either foam density or foam stability. Dilational parameters at CMC suggest slow bubble stabilization resulting in large bubble size but excellent foam stability, which was verified by foaming experiments by air sparging at 10 CMC. Comparison with $C_{12}E_5$ and $C_{12}Glc_2$ confirmed the trend that high ω_0 enhances small bubble stabilization and high ε_0 enhances foam stability. The nature of polar heads support the fact that the presence of intermolecular H-bonds strength accounts for the surface elastic behaviour.[22–25,30,57,58] Indeed, $C_{12}Gly_2$ and $C_{12}Glc_2$ present the most densely packed air/water interfaces, the highest elasticity limits and the highest number of hydroxyl groups per molecule (7 for $C_{12}Glc_2$ and 3 for $C_{12}Gly_2$, compared to 1 in $C_{12}E_5$). The main foam destabilization phenomenon was identified to be bubble coalescence, which rate was similar in the case of $C_{12}Gly_2$ and $C_{12}Glc_2$ but was initially faster for $C_{12}E_5$ until total foam break.

Further precision on high frequency elasticity limit ε_0 could be obtained using equipment able to reach higher oscillation frequency such as the capillary pressure tensiometer (CPT) reaching frequencies up to 100 Hz.[59] For some applications, using $C_{12}Gly_2$ as foaming agent would require overcoming its high initial bubble size. This could be investigated by varying the bubble generation process, e.g. by reducing the air flow (not possible with our equipment) or nucleating gas bubbles from the solution by gas dissolution.[1] Another idea could be to use this surfactant in combination with a quickly diffusing surfactant so as to associate the quick bubble stabilization and the long-term interface stabilization.

Acknowledgements

Chevreul Institute (FR 2638), Ministère de l'Enseignement Supérieur et de la Recherche, Région Hauts-de-France, and FEDER are acknowledged for supporting and funding partially this work. We are deeply grateful to Dr. Leila Monnier who kindly helped us at the beginning of the measurements with the TECLIS tensiometer and updated the protocols for its use. Finally, we also thank to Naila Dami who performed the experiments requested by reviewers (influence of the protocol on the size of the aggregates).

Supporting Information

SI 1. NMR spectra

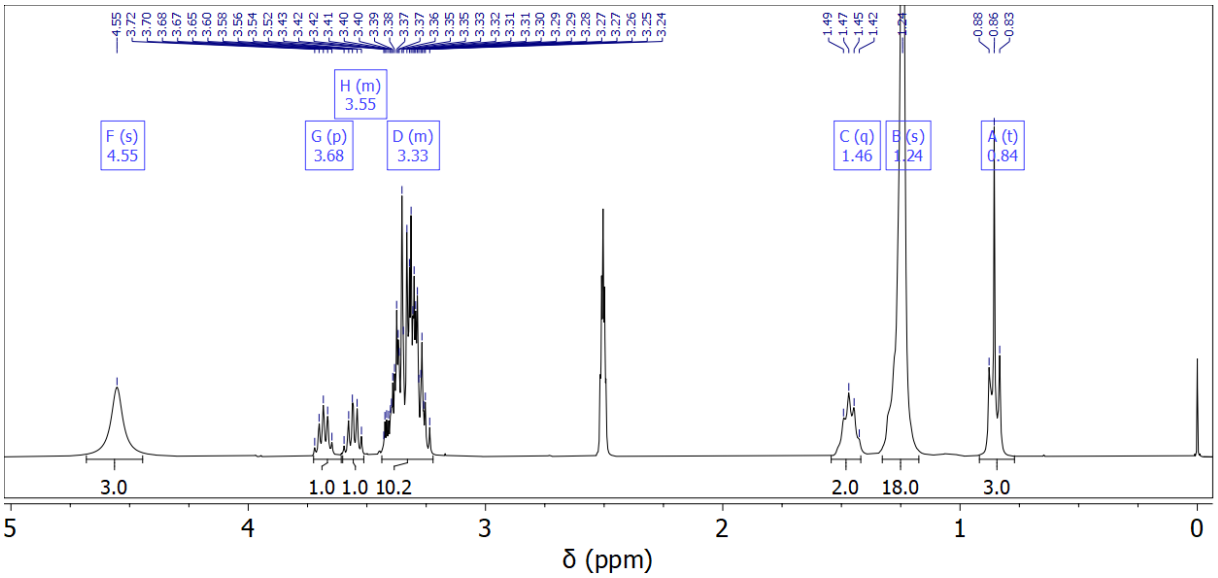

Figure S1. ^{1}H NMR (300 MHz) spectrum of 1-*O*-dodecyl diglyceryl ether in d_6-DMSO. Peak at 2.5 ppm corresponds to the solvent peak.

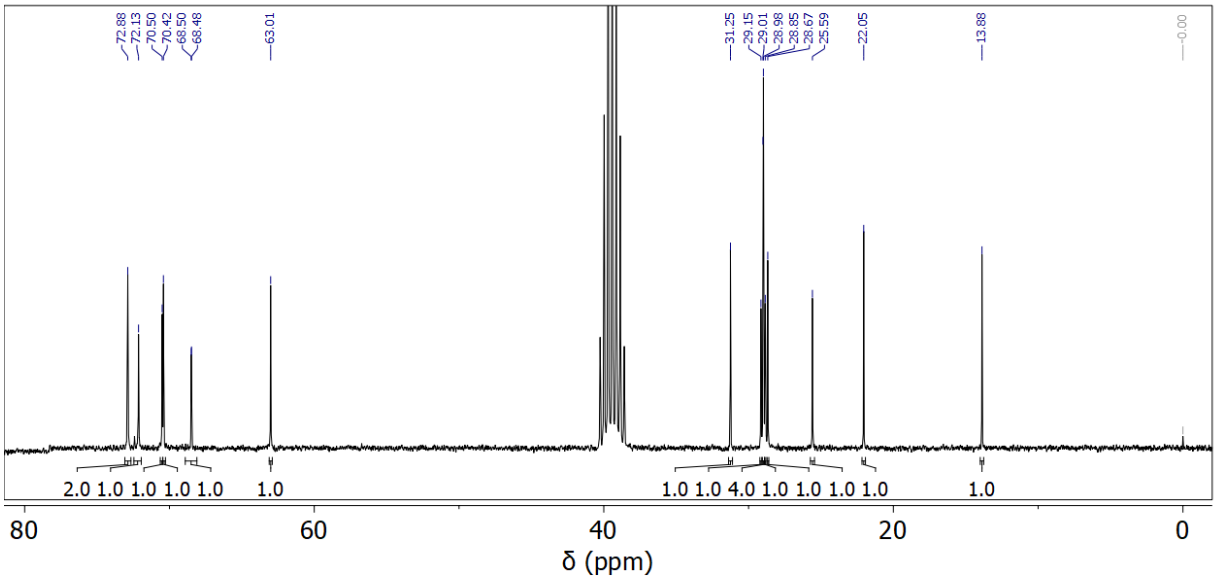

Figure S2. ^{13}C NMR (75 MHz) spectrum of 1-*O*-dodecyl diglyceryl ether in d_6-DMSO. Peaks around 40 ppm corresponds to the solvent peak.

SI 2. Isotherm Fitting Models

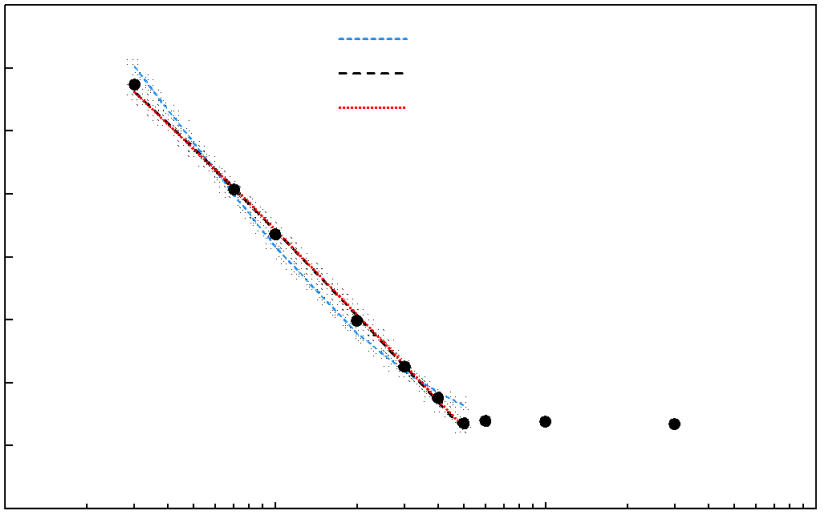

Figure S3. Surface tension isotherm of $C_{12}Gly_2$ at 25.0 °C. Data before CMC is fitted with either Henry, Langmuir-Szyszkowski, or Frumkin surface equations of state.

Table S1. Parameters for Frumkin and Henry surface equations of state for surface tension isotherm of $C_{12}Gly_2$ at 25°C.

Model	Equation	Parameters
Henry	$\gamma = \gamma_0 - RT\Gamma_\infty \frac{c}{a+c}$	$\Gamma\infty$= 1.98×10^{-5} mol.m^{-2} a = 5.61×10^{-6} mol.L^{-1}
Langmuir-Szyskowski	$\gamma = \gamma_0 - RT\Gamma_\infty \ln ln \left(1 + \frac{c}{a}\right)$	$\Gamma\infty$= 4.08×10^{-6} mol.m^{-2} a = 5.35×10^{-7} mol.L^{-1}
Frumkin	$\gamma = \gamma_0 - RT\Gamma_\infty (ln(1 + \frac{c}{a}) + \frac{\beta}{2}(\frac{c}{a+c})^2)$	$\Gamma\infty$= 4.05×10^{-6} mol.m^{-2} ^{a} = 5.35×10^{-7} mol.L^{-1} β= 0.04

SI 3. Influence of agitation protocol and temperature in the size distribution (1×10^{-3} M)

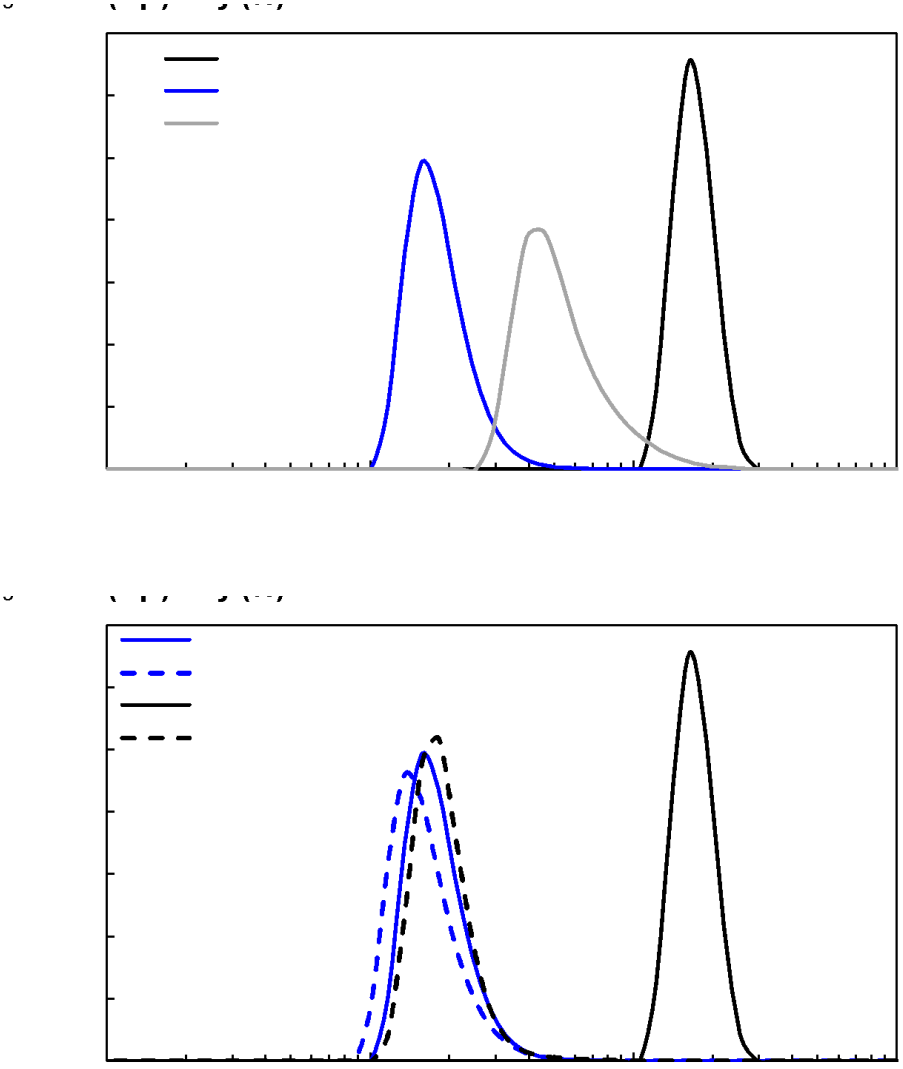

Figure S4. Aggregate size distribution in $C_{12}Gly_2$ 1×10^{-3} M solution measured by DLS A) Influence of different agitation protocols at 25°C: 1h30 of magnetic stirring at 750 rpm (black); the same protocol followed by 1m30s of solutions (blue) and the standard protocol of 30 min in ultrasonic bath (gray). B) Influence of Temperature. Dotted lines correspond to 40°C experiments.

SI 4. Influence of temperature on the structures observed by Optical microscopy (1.5×10^{-2} M)

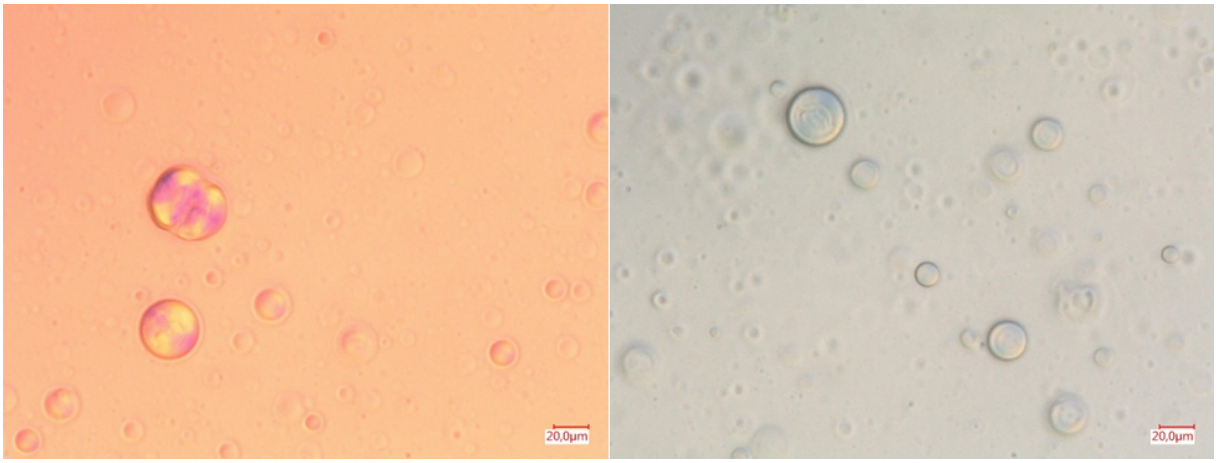

Figure S5. Optical microscope observations of $C_{12}Gly_2$ aqueous solution (1.5×10^{-2} M) at 60°C.

SI 5. Comparison in the different methods to calculate ε_0 and ω_0

A comparison was done in Table S2 between ε_0 and ω_0 values determined either by fitting equations (10) and (11) (method A) or by calculating and averaging ε_0 and ω_0 values for each frequency according to equations (8) and (9) (method B). It shows that both methods coincide with each other except for $C_{12}E_5$ at 1 CMC, for which the fitted values (method A) are not consistent with the expected ε_0 evolution with concentration.

Table S2. High frequency limit of dilational surface elasticity ε_0 ($mN.m^{-1}$) and molecular exchange parameter ω_0 ($rad.s^{-1}$) values for $C_{12}Gly_2$ and $C_{12}E_5$ at 0.1 CMC, 0.5 CMC and 1 CMC calculated by fitting the data (method A) or by averaging the ε_0 and ω_0 values calculated at each frequency (method B).

		0.1 CMC		0.5 CMC		1 CMC	
		ε_0 ($mN.m^{-1}$)	ω_0 ($rad.s^{-1}$)	ε_0 ($mN.m^{-1}$)	ω_0 ($rad.s^{-1}$)	ε_0 ($mN.m^{-1}$)	ω_0 ($rad.s^{-1}$)
$C_{12}Gly_2$	A	64.6 ± 1.2	0.024 ± 0.007	85.5 ± 1.4	0.49 ± 0.05	127.5 ± 6.2	12.8 ± 1.7
	B	64.5 ± 1.5	0.043 ± 0.005	97.7 ± 3.3	0.89 ± 0.14	125.6 ± 22.5	13.0 ± 5.8
$C_{12}E_5$	A	67.3 ± 0.4	0.118 ± 0.005	67.3 ± 1.5	2.1 ± 0.2	40.7 ± 5.1	8.5 ± 2.7
	B	67.2 ± 3.0	0.11 ± 0.06	75.1 ± 7.3	3.1 ± 0.8	84.6 ± 5.8	44.8 ± 10.8

References

[1] R.J. Pugh, Foaming, foam films, antifoaming and defoaming, Adv. Colloid Interface Sci. 64 (1996) 67–142. https://doi.org/10.1016/0001-8686(95)00280-4.

[2] A. Prins, Surface Rheology and Practical Behaviour of Foams and Thin Liquid Films, Chem. Ing. Tech. 64 (1992) 73–75. https://doi.org/10.1002/cite.330640116.

[3] Th. Engels, W. von Rybinski, P. Schmiedel, Structure and dynamics of surfactant-based foams, in: H. Rehage, G. Peschel (Eds.), Structure, Dynamics and Properties of Disperse Colloidal Systems, Steinkopff, Darmstadt, 1998: pp. 117–126.

[4] N. Denkov, S. Tcholakova, N. Politova-Brinkova, Physicochemical control of foam properties, Curr. Opin. Colloid Interf. Sci. 50 (2020) 101376. https://doi.org/10.1016/j.cocis.2020.08.001.

[5] B. Petkova, S. Tcholakova, N. Denkov, Foamability of surfactant solutions: Interplay between adsorption and hydrodynamic conditions, Colloids Surf. A Physicochem. Eng. Asp. 626 (2021) 127009. https://doi.org/10.1016/j.colsurfa.2021.127009.

[6] M.J. Rosen, J.T. Kunjappu, Foaming and Antifoaming by Aqueous Solutions of Surfactants, in: Surfactants and Interfacial Phenomena, 4th ed., John Wiley & Sons, Ltd, 2012: pp. 308–335. https://doi.org/10.1002/9781118228920.ch7.

[7] J.F. Sadoc, N. Rivier, eds., Foams and Emulsions, Kluwer Academic, Dordrecht, 1999. http://link.springer.com/book/10.1007/978-94-015-9157-7.

[8] D. Exerowa, P.M. Kruglyakov, Foam and Foam Films: Theory, Experiment, Application, 1st edition, Elsevier Science, Amsterdam; New York, 1997.

[9] A.J. Wilson, Experimental Techniques for the Characterization of Foams, in: R.K. Prud'homme, S.A. Khan (Eds.), Foams: Theory Measurements, and Applications, 1st ed., M. Dekker, New York, 1996.

[10] S. Tcholakova, Z. Mitrinova, K. Golemanov, N.D. Denkov, M. Vethamuthu, K.P. Anathapadmanabhan, Control of Ostwald Ripening by Using Surfactants with High Surface Modulus., Langmuir. 27 (2011) 14807–14819. https://doi.org/10.1021/la203952p.

[11] C. Stubenrauch, R. Miller, Stability of Foam Films and Surface Rheology: An Oscillating Bubble Study at Low Frequencies, J. Phys. Chem. B. 108 (2004) 6412–6421. https://doi.org/10.1021/jp049694e.

[12] E. Santini, F. Ravera, M. Ferrari, C. Stubenrauch, A. Makievski, J. Krägel, A surface rheological study of non-ionic surfactants at the water–air interface and the stability of the corresponding thin foam films, Colloids Surf. A Physicochem. Eng. Asp. 298 (2007) 12–21. https://doi.org/10.1016/j.colsurfa.2006.12.004.

[13] S.E. Friberg, C. Solans, Surfactant association structures and the stability of emulsions and foams, Langmuir. 2 (1986) 121–126. https://doi.org/10.1021/la00068a001.

[14] S.E. Friberg, Foams from non-aqueous systems, Curr. Opin. Colloid Interf. Sci. 15 (2010) 359–364. https://doi.org/10.1016/j.cocis.2010.05.011.

[15] L.K. Shrestha, D.P. Acharya, S.C. Sharma, K. Aramaki, H. Asaoka, K. Ihara, T. Tsunehiro, H. Kunieda, Aqueous foam stabilized by dispersed surfactant solid and lamellar liquid crystalline phase, J. Colloid Interface Sci. 301 (2006) 274–281. https://doi.org/10.1016/j.jcis.2006.04.065.

[16] L.K. Shrestha, E. Saito, R.G. Shrestha, H. Kato, Y. Takase, K. Aramaki, Foam stabilized by dispersed surfactant solid and lamellar liquid crystal in aqueous systems of diglycerol fatty acid esters, Colloids Surf. A Physicochem. Eng. Asp. 293 (2007) 262–271. https://doi.org/10.1016/j.colsurfa.2006.07.054.

[17] H. Kunieda, L.K. Shrestha, D.P. Acharya, H. Kato, Y. Takase, J.M. Gutiérrez, Super-Stable Nonaqueous Foams in Diglycerol Fatty Acid Esters—Non Polar Oil Systems, J. Dispers. Sci. Technol. 28 (2007) 133–142. https://doi.org/10.1080/01932690600992779.

[18] Y. Shi, W. Dayoub, A. Favre-Réguillon, G.-R. Chen, M. Lemaire, Straightforward selective synthesis of linear 1-O-alkyl glycerol and di-glycerol monoethers, Tetrahedron Lett. 50 (2009) 6891–6893. https://doi.org/10.1016/j.tetlet.2009.09.134.

[19] H. Sagitani, Y. Hayashi, M. Ochiai, Solution properties of homogeneous polyglycerol dodecyl ether nonionic surfactants, JAOCS. 66 (1989) 146–152. https://doi.org/10.1007/BF02661806.
[20] L.K. Shrestha, R.G. Shrestha, T. Iwanaga, K. Aramaki, Aqueous Phase Behavior of Diglycerol Fatty Acid Esters, J. Dispers. Sci. Technol. 28 (2007) 883–891. https://doi.org/10.1080/01932690701459538.
[21] L. Delforce, J.F. Ontiveros, V. Nardello-Rataj, J.-M. Aubry, Rational design of O/W nanoemulsions based on the surfactant dodecyldiglyceryl ether using the normalized HLD concept and the formulation-composition map, Colloids Surf. A Physicochem. Eng. Asp. 671 (2023) 131679. https://doi.org/10.1016/j.colsurfa.2023.131679.
[22] C. Stubenrauch, L.K. Shrestha, D. Varade, I. Johansson, G. Olanya, K. Aramaki, P. Claesson, Aqueous Foams Stabilized by n-Dodecyl-β-D-Maltoside, Hexaethyleneglycol Monododecyl Ether, and Their 1: 1 Mixture, Soft Matter. 5 (2009) 3070–3080. https://doi.org/10.1039/B903125A.
[23] C. Stubenrauch, M. Hamann, N. Preisig, V. Chauhan, R. Bordes, On how hydrogen bonds affect foam stability, Adv. Colloid Interface Sci. 247 (2017) 435–443. https://doi.org/10.1016/j.cis.2017.02.002.
[24] C. Stubenrauch, P.M. Claesson, M. Rutland, E. Manev, I. Johansson, J.S. Pedersen, D. Langevin, D. Blunk, C.D. Bain, Mixtures of n-Dodecyl-β-D-Maltoside and Hexaoxyethylene Dodecyl Ether - Surface Properties, Bulk Properties, Foam Films, and Foams, Adv. Colloid Interface Sci. 155 (2010) 5–18. https://doi.org/10.1016/j.cis.2009.12.002.
[25] J. Boos, W. Drenckhan, C. Stubenrauch, Protocol for Studying Aqueous Foams Stabilized by Surfactant Mixtures, J. Surfact. Deterg. 16 (2013) 1–12. https://doi.org/10.1007/s11743-012-1416-2.
[26] L. Saulnier, J. Boos, C. Stubenrauch, E. Rio, Comparison between generations of foams and single vertical films – single and mixed surfactant systems, Soft Matter. 10 (2014) 5280–5288. https://doi.org/10.1039/C4SM00326H.
[27] E. Carey, C. Stubenrauch, Foaming properties of mixtures of a non-ionic (C12DMPO) and an ionic surfactant (C12TAB), J. Colloid Interface Sci. 346 (2010) 414–423. https://doi.org/10.1016/j.jcis.2010.03.013.
[28] E. Carey, C. Stubenrauch, Free drainage of aqueous foams stabilized by mixtures of a non-ionic (C12DMPO) and an ionic (C12TAB) surfactant, Colloids Surf. A Physicochem. Eng. Asp. 419 (2013) 7–14. https://doi.org/10.1016/j.colsurfa.2012.11.037.
[29] N. Raykundaliya, R. Bordes, K. Holmberg, J. Wu, P. Somasundaran, D.O. Shah, The Effect on Solution Properties of Replacing a Hydrogen Atom with a Methyl Group in a Surfactant, Tenside Surfactant Deter. 52 (2015) 369–374. https://doi.org/10.3139/113.110387.
[30] K. Schellmann, N. Preisig, P. Claesson, C. Stubenrauch, Effects of Protonation on Foaming Properties of Dodecyldimethylamine Oxide Solutions: A pH-Study, Soft Matter. 11 (2015) 561–571. https://doi.org/10.1039/C4SM02476A.
[31] J.R. Kanicky, A.F. Poniatowski, N.R. Mehta, D.O. Shah, Cooperativity among Molecules at Interfaces in Relation to Various Technological Processes: Effect of Chain Length on the pKa of Fatty Acid Salt Solutions, Langmuir. 16 (2000) 172–177. https://doi.org/10.1021/la990719o.
[32] W.C. Griffin, Calculation of HLB values of non-ionic surfactants, J. Soc. Cosmet. Chem. 5 (1954) 249–256.
[33] J.F. Ontiveros, C. Pierlot, M. Catté, V. Molinier, J.-L. Salager, J.-M. Aubry, Structure–interfacial properties relationship and quantification of the amphiphilicity of well-defined ionic and non-ionic surfactants using the PIT-slope method, J. Colloid Interface Sci. 448 (2015) 222–230. https://doi.org/10.1016/j.jcis.2015.02.028.
[34] C. Stubenrauch, J. Schlarmann, R. Strey, A disjoining pressure study of n-dodecyl-β-D-maltoside foam films, Phys. Chem. Chem. Phys. 4 (2002) 4504–4513. https://doi.org/10.1039/B205728J.

[35] J. Schlarmann, C. Stubenrauch, Stabilization of foam films with non-ionic surfactants: Alkyl polyglycol ethers compared with alkyl polyglucosides, Tenside Surfactant Deter. 40 (2003) 190–195.
[36] B.W. Berger, R.Y. García, A.M. Lenhoff, E.W. Kaler, C.R. Robinson, Relating Surfactant Properties to Activity and Solubilization of the Human Adenosine A3 Receptor, Biophys. J. 89 (2005) 452–464. https://doi.org/10.1529/biophysj.104.051417.
[37] J. Boos, N. Preisig, C. Stubenrauch, Dilational Surface Rheology Studies of n-Dodecyl-β-D-Maltoside, Hexaoxyethylene Dodecyl Ether, and Their 1:1 Mixture, Adv. Colloid Interface Sci. 197–198 (2013) 108–117. https://doi.org/10.1016/j.cis.2013.05.001.
[38] C.-H. Chang, E.I. Franses, Adsorption dynamics of surfactants at the air/water interface: a critical review of mathematical models, data, and mechanisms, Colloids Surf. A Physicochem. Eng. Asp. 100 (1995) 1–45. https://doi.org/10.1016/0927-7757(94)03061-4.
[39] J. Lucassen, M. Van den Tempel, Longitudinal waves on visco-elastic surfaces, J. Colloid Interface Sci. 41 (1972) 491–498. https://doi.org/10.1016/0021-9797(72)90373-6.
[40] J. Lucassen, M. Van den Tempel, Dynamic measurements of dilational properties of a liquid interface, Chem. Eng. Sci. 27 (1972) 1283–1291. https://doi.org/10.1016/0009-2509(72)80104-0.
[41] D.J. Mitchell, G.J.T. Tiddy, L. Waring, T. Bostock, M.P. McDonald, Phase behaviour of polyoxyethylene surfactants with water. Mesophase structures and partial miscibility (cloud points), J. Chem. Soc., Faraday Trans. 1. 79 (1983) 975–1000. https://doi.org/10.1039/F19837900975.
[42] R. Strey, R. Schomäcker, D. Roux, F. Nallet, U. Olsson, Dilute lamellar and L3 phases in the binary water–C12E5 system, J. Chem. Soc., Faraday Trans. 86 (1990) 2253–2261. https://doi.org/10.1039/FT9908602253.
[43] G.G. Warr, C.J. Drummond, F. Grieser, B.W. Ninham, D.F. Evans, Aqueous Solution Properties of Nonionic n-Dodecyl-β-D-Maltoside Micelles, J. Phys. Chem. 90 (1986) 4581–4586. https://doi.org/10.1021/j100410a022.
[44] M. Hishida, K. Tanaka, Transition of the hydration state of a surfactant accompanying structural transitions of self-assembled aggregates, J. Phys.: Condens. Matter. 24 (2012) 284113. https://doi.org/10.1088/0953-8984/24/28/284113.
[45] P. Izquierdo, D.P. Acharya, K. Hirayama, H. Asaoka, K. Ihara, T. Tsunehiro, Y. Shimada, Y. Asano, S. Kokubo, H. Kunieda, Phase Behavior of Pentaglycerol Monostearic and Monooleic Acid Esters in Water, J. Dispers. Sci. Technol. 27 (2006) 99–103. https://doi.org/10.1081/DIS-200066805.
[46] M.J. Rosen, A.W. Cohen, M. Dahanayake, X.Y. Hua, Relationship of structure to properties in surfactants. 10. Surface and thermodynamic properties of 2-dodecyloxypoly(ethenoxyethanol)s, C12H25(OC2H4)xOH, in aqueous solution, J. Phys. Chem. 86 (1982) 541–545. https://doi.org/10.1021/j100393a025.
[47] C.J. Drummond, G.G. Warr, F. Grieser, B.W. Ninham, D.F. Evans, Surface Properties and Micellar Interfacial Microenvironment of n-Dodecyl-β-D-Maltoside, J. Phys. Chem. 89 (1985) 2103–2109. https://doi.org/10.1021/j100256a060.
[48] K. Shinoda, T. Yamaguchi, R. Hori, The Surface Tension and the Critical Micelle Concentration in Aqueous Solution of β-D-Alkyl Glucosides and their Mixtures, BCSJ. 34 (1961) 237–241. https://doi.org/10.1246/bcsj.34.237.
[49] T. Kato, T. Nakamura, M. Yamashita, M. Kawaguchi, T. Kato, T. Itoh, Surfactant properties of purified polyglycerol monolaurates, J. Surfact. Deterg. 6 (2003) 331–337. https://doi.org/10.1007/s11743-003-0278-x.
[50] Y. Jayalakshmi, L. Ozanne, D. Langevin, Viscoelasticity of Surfactant Monolayers, J. Colloid Interface Sci. 170 (1995) 358–366. https://doi.org/10.1006/jcis.1995.1113.
[51] D. Georgieva, A. Cagna, D. Langevin, Link between surface elasticity and foam stability, Soft Matter. 5 (2009) 2063–2071. https://doi.org/10.1039/B822568K.

[52] E.H. Lucassen-Reynders, Anionic surfactants: Physical chemistry of surfactant action, M. Dekker, New York, 1981.
[53] V. Bergeron, Disjoining Pressures and Film Stability of Alkyltrimethylammonium Bromide Foam Films, Langmuir. 13 (1997) 3474–3482. https://doi.org/10.1021/la970004q.
[54] D. Langevin, Influence of interfacial rheology on foam and emulsion properties, Adv. Colloid Interface Sci. 88 (2000) 209–222. https://doi.org/10.1016/s0001-8686(00)00045-2.
[55] V. Bergeron, Forces and structure in thin liquid soap films, J. Phys.: Condens. Matter. 11 (1999) R215–R238. https://doi.org/10.1088/0953-8984/11/19/201.
[56] A.A. Sonin, A. Bonfillon, D. Langevin, Thinning of Soap Films: The Role of Surface Viscoelasticity, J. Colloid Interface Sci. 162 (1994) 323–330. https://doi.org/10.1006/jcis.1994.1046.
[57] M. Kanduč, E. Schneck, C. Stubenrauch, Intersurfactant H-Bonds Between Head Groups of n-Dodecyl-β-D-Maltoside at the Air-Water Interface, J. Colloid Interface Sci. 586 (2021) 588–595. https://doi.org/10.1016/j.jcis.2020.10.125.
[58] D. Ranieri, N. Preisig, C. Stubenrauch, On the Influence of Intersurfactant H-Bonds on Foam Stability: A Study with Technical Grade Surfactants, TSD. 55 (2018) 6–16. https://doi.org/10.3139/113.110537.
[59] F. Ravera, M. Ferrari, E. Santini, L. Liggieri, Influence of surface processes on the dilational visco-elasticity of surfactant solutions, Adv. Colloid Interface Sci. 117 (2005) 75–100. https://doi.org/10.1016/j.cis.2005.06.002.